Accepted Manuscript

Effect of dynamic storage temperatures on the microstructure of frozen carrot imaged using X-ray micro-CT

Victor Vicent, Fatou-Toutie Ndoye, Pieter Verboven, Bart Nicolaï, Graciela Alvarez

PII: S0260-8774(18)30497-7

DOI: https://doi.org/10.1016/j.jfoodeng.2018.11.015

Reference: JFOE 9466

To appear in: *Journal of Food Engineering*

Received Date: 6 July 2018

Revised Date: 6 October 2018

Accepted Date: 15 November 2018

Please cite this article as: Vicent, V., Ndoye, F.-T., Verboven, P., Nicolaï, B., Alvarez, G., Effect of dynamic storage temperatures on the microstructure of frozen carrot imaged using X-ray micro-CT, *Journal of Food Engineering* (2018), doi: https://doi.org/10.1016/j.jfoodeng.2018.11.015.

Effect of dynamic storage temperatures on the microstructure of frozen carrot imaged using X-ray micro-CT

Victor Vicent[a,b], Fatou-Toutie Ndoye[a,*], Pieter Verboven[b], Bart Nicolaï[b], Graciela Alvarez[a]

[a]*IRSTEA, Refrigeration Processes Engineering Research Unit, 1, rue Pierre-Gilles de Gennes, 92761, Antony, France*

[b]*BIOSYST-MeBioS, KU Leuven, Willem de Croylaan 42, B-3001 Leuven, Belgium*

[*]**Corresponding author**: email: fatou-toutie.ndoye@irstea.fr

Abstract

Frozen vegetables are often exposed to dynamic temperature conditions during cold storage and distribution chain. The resulting ice recrystallization leads to microstructural changes, which is directly linked to the final vegetable quality. To this end, X-ray µCT was applied to visualize and quantify 3D ice crystal changes in carrot over a period of two months of frozen storage with dynamically changing temperature. The studied conditions revealed a significant increase in ice crystal size during the storage period. The equivalent diameter of the ice crystals increased from 246 ± 15.9 µm, to 342 ± 13.2 µm, 394 ± 18.5 µm, 525 ± 28.0 µm and 578 ± 27.6 µm at 0 d, 7 d, 14 d, 30 d and 60 d of storage, respectively, while the number of ice crystals decreased. The 3D data on the ice crystals and image analysis presented within this paper provide an insight making it possible to describe microstructure evolution, and for better control cold storage sector of frozen vegetables.

Keywords: Cold chain, ice recrystallization, X-ray µCT, image analysis, 3D microstructure

1. Introduction

Carrots (*Daucus carota* L.) are good sources of carotenoids and dietary fibers, which are functional components having substantial health-promoting properties. Carrots are perishable root vegetables because of their high-water content. Furthermore, carrot tissue comprises different layers: parenchyma cells, vascular tissue and peripheral cortex tissue of different sizes and shapes. Carrot tissue structure is affected by vascular bundle growth (Voda et al., 2012). One of the greatest challenges for the frozen food industry is to preserve the quality of food materials during extended storage for consumer's convenience.

Food-processing operations, including freezing and frozen storage, may change the tissue structure significantly (Aguilera and Stanley, 1999; Ullah et al., 2014). During freezing, ice crystals are formed throughout the cellular structure. The formation of ice crystals can modify the tissue microstructure of plant-based materials (Mousavi et al., 2007; Vicent et al., 2017). During subsequent storage, ice recrystallization occurs, involving ice crystals resizing and redistribution (Ullah et al., 2014; Ndoye and Alvarez, 2015), resulting in further microstructural changes. Small crystals are thermodynamically less stable due to a high surface to volume ratio, implying that small crystals can easily melt and the released water molecules are deposited on the surface of the larger crystals (Donhowe and Hartel, 1996; Hartel, 1998; Pronk et al., 2005; Hagiwara et al., 2006). Larger crystals thus tend to increase in size at the expense of small crystals. Pronk et al. (2005) commented that in food materials, Ostwald ripening is a main mechanism for ice recrystallization compared with other mechanisms, including iso-mass and accretion recrystallization. Recrystallization is more likely to occur if frozen food undergoes temperature abuse, such as dynamic temperatures during frozen storage and within the distribution chain (Zaritzky, 2000). Enlargement of ice crystals can occur at a constant temperature during long-term storage, especially in a liquid state, i.e., at a temperature beyond glass transition temperature where molecular mobility is

increased (Donhowe and Hartel, 1996; Syamaladevi et al., 2012). Ice crystal growth is strongly linked to food microstructural changes that often affect the stability and quality of fruit and vegetables, and these changes include alteration in texture, sensory quality and nutritional values (Zaritzky, 2000; Ho et al., 2013). In frozen vegetables, Gonçalves et al. (2011a, 2011b) worked with broccoli and pumpkin, respectively during frozen storage. Both studies reported irreversible changes of quality, such as drip loss, sensory and textural changes as well as nutritional loss as a result of ice crystal growth. Vicent et al. (2018) recently showed changes of quality such as drip loss in frozen apple tissue as a result of ice recrystallization during storage with temperature fluctuations. Therefore, the need to investigate the microstructural changes in 3D data sets is preferable, and could help to elucidate the quality and stability changes occurring in vegetables.

X-ray micro-computed tomography (X-ray µCT) has become popular as a 3D imaging technique to visualize and quantify the internal microstructure features of frozen vegetables (Mousavi et al., 2007; Voda et al., 2012; Ullah et al., 2014; Zhao and Takhar, 2017). However, most of the studies conducted in the past have focused only on the visualization of the microstructure of frozen foods after a freeze-drying process to lyophilize frozen water. Mousavi et al. (2007) used X-ray µCT to investigate the 3D ice crystals during freezing of different food products, including carrots, and stated that ice crystals varied in sizes according to the freezing rates applied. Ullah et al. (2014) applied X-ray µCT to visualize ice recrystallization in frozen potatoes during storage with temperature fluctuations, and reported the ice crystals increased in size with the increase in amplitude of temperature fluctuations. Zhao and Takhar (2017) also used X-ray µCT to study ice recrystallization phenomena in frozen potatoes subjected to different temperature fluctuations during storage. However, Mousavi et al. (2007), Ullah et al. (2014) and Zhao and Takhar (2017) assumed that the void structures formed in the freeze-dried products represented the ice crystal morphology. In fact,

the freeze-drying process may have changed frozen-food structures investigated through shrinkage (Voda et al., 2012), leading to inconclusive results. To circumvent this issue, Vicent et al. (2017) developed and validated an X-ray µCT imaging procedure directly on frozen samples to investigate the 3D microstructure of ice crystals in apple tissue at a low temperature (-18 ^{o}C). The method employed prior knowledge by incorporating X-ray attenuation coefficients of reference samples into the image analysis. The method remains to be tested to determine whether it is suitable for investigating the relationship between the 3D microstructure of the ice crystals and the storage temperature without requiring a freeze-drying step.

The objective of this study was to quantify for the first time 3D ice crystal growth in frozen carrots stored over a period of two months at dynamically changing temperature by performing image analysis using the X-ray attenuation coefficients of reference model samples. The imaging methodology elaborated by Vicent et al. (2017) was implemented in order to study the ice crystal propagation due to ice recrystallization.

2. Materials and methods

2.1 Carrot sample and preparation

Carrots (*Daucus carota* L., cv. Nantesa) were purchased from a local supplier in Paris, France, and were of different sizes (diameter: 2 to 4 cm; length: 14 to 20 cm). Prior to sample preparation, the carrots were washed and stored at 4 °C overnight to equilibrate. Cylindrical tissue samples with a height of 14 mm were excised from carrot tissue by using a cork bore with an inner diameter of 6 mm as illustrated in Fig. 1a-b. Subsequently, each excised sample was placed in a straw to facilitate the mounting of samples onto the cooling stage for image acquisition using X-ray µCT. Next, five replicate carrot samples were numbered and packed in two plastic bags for the freezing process and subsequent storage experiment.

2.2 Sample freezing

The prepared samples were frozen in an air blast freezer set at a temperature of -33 °C. The sample and freezer temperatures were recorded during freezing using calibrated thermocouples (type T thermocouple of 0.2 mm) attached to a data logger system (34970A, Agilent HP, Santa Clara, USA) connected to a computer. For sample temperature records, a thermocouple was inserted into a sample core of the representative bag. The air freezer temperature was recorded as well. Freezing was completed when the sample core temperature reached -18 ^{o}C. Fig. 2 shows the temperature profile during the freezing process; a typical cooling step is observed whereby the sample temperature was reduced to the freezing point, during which sensible heat was removed from the carrot tissue samples. Next is a super-cooling step during which the temperature falls below the freezing point. Subsequently, the freezing period started, in which liquid water within carrot tissue was converted into ice accompanied by latent heat removal as the temperature decreased gradually. Finally, the carrot temperature decreased until the desired final temperature of -18 ^{o}C was reached; during this step sensible heat was removed. As a result, an overall freezing rate of approximately 9.1 ^{o}C per min was achieved. The rate of freezing was estimated from the ratio of the temperature difference between ambient temperature (20 ^{o}C) and the freezing temperature (-18 ^{o}C) divided by the time difference from ambient temperature to freezing temperature as defined by the International Institute of Refrigeration (Bogh-Sorensen, 2006).

2.3 Dynamic change of storage temperatures

Frozen samples were stored under dynamic change of temperature conditions using two freezers. Samples were held in the first freezer set at a temperature of -18 ^{o}C for 23 h and then moved to a second freezer set at a temperature of -5 ^{o}C for 1 h, as shown in Fig. 1c. The dynamic temperature cycle was performed daily over a period of two months, with the exception of weekends. This storage scenario made it possible to study the effects of the poor

practice in terms of temperature dynamic conditions that could occur during frozen storage. At sub-zero temperatures, the glass transition temperature (T_g') is an important reference temperature to describe quality and storability of food materials. During glass transition, the mechanical properties of the product change from those of an elastic material to those of a brittle one due to changes in molecular mobility. This causes a step change in heat capacity of the product. It should be noted that the transition does not occur suddenly at a single temperature but rather over a range of temperature. T_g' is then estimated from the temperature in the middle of the step region. Reid et al. (2003) measured the T_g' in several food materials using Differential Scanning Calorimetry (DSC). Gonçalves et al. (2007) also determined the glass transition temperature (T_g') in different vegetables, includes carrot using DSC technique. The authors stated a T_g' value to be approximately -32 ^{o}C in carrot. This indicates that no amorphous solid phase in the frozen carrot tissue was formed during freezing and dynamic storage experiments.

2.4 Attenuation coefficient references

In tomographic images, the grey value does correspond to the linear attenuation coefficient that describes the fraction of the X-rays absorbed or scattered relatively to the material properties, including density. The correlations are often inadequate when attempting to accurately classify distinctive components in the X-ray images. This is because food components consist of elements with comparable atomic numbers, and the X-rays applied are polychromatic. This is mainly the case here when segmenting pure ice and unfrozen-matrix. Within this framework and according to the imaging method developed by Vicent et al. (2017), two reference samples were scanned and analyzed at the same settings as the frozen carrot samples: (i) frozen distilled water was used to identify the X-ray attenuation coefficients of pure ice crystals in frozen carrot; (ii) concentrated carrot juice was examined to represent the X-ray attenuation coefficient of the unfrozen-matrix in frozen carrot tissue. As

147 such, concentrated carrot juice (68 % Brix) was prepared from carrot tissue juice (9 % Brix)
148 using a rotary evaporator (RE400, Staffordshire, ST15 OSA, UK) at 60 ± 4 ^{o}C. The
149 concentrated juice was stored at a temperature of -18 ^{o}C and assumed to have a similar
150 concentration as the unfrozen matrix in frozen carrot tissue at -18 ^{o}C.

151 **2.5 X-ray µCT imaging**

152 X-ray µCT scans of frozen carrot samples were acquired using high-resolution X-ray micro-
153 computed tomography (DeskTom RX 130, Chavanod, France). The frozen sample at -18 ^{o}C
154 was gently placed into a cooling stage cylinder; this cooling stage was made of phase change
155 material (PCM) designed to maintain the sample temperature during the entire scanning
156 protocol. PCM consisted of NaCL (25 % w/w) and commercial blend gum (5 % w/w)
157 (Germantown Premium IC Blend, Danisco) was used. To isolate both the samples and PCM
158 from the environment, the cooling stage was surrounded by and covered with polystyrene
159 foam. From preliminary test, the use of PCM together with polystyrene foam during imaging
160 was sufficient to minimize the temperature difference to 2 °C, i.e., from -18 to -16 ^{o}C during
161 the entire scanning duration. An X-ray tube voltage of 60 kV was applied to capture 896
162 projection images with an exposure time of 0.2 s per projection. A voxel resolution of 8.9 µm
163 was used for image acquisition. The projection images were recorded over a 360^{o} rotation
164 with a step size of 0.4^{o} and required a total scanning time of 11 min per sample. After each
165 scan, the sample was placed back in the freezer set at a temperature of -18 ^{o}C for sequential
166 storage. This enabled us to follow the microstructural changes for the same carrot sample
167 throughout the storage experiment.

168 XAct 2 software (RX Solution SAS, Chavanod, France) was utilized to reconstruct the 3D
169 image from a series of X-ray radiograph projections using the filtered back-projection
170 algorithm (Feldkamp et al., 1984). Noise filtering and phase contrast correction were applied
171 to improve image quality. Reconstructed images were converted to 8-bit precision to reduce

the computational load during image processing. The scanning and reconstruction procedures outlined above were utilized to acquire CT images of frozen carrot at each time point during storage and were also used for the reference samples.

Fresh carrot scans were acquired using a SkyScan 1172 high-resolution desktop X-ray μCT (Bruker micro CT, Kontich, Belgium) at a voxel resolution of 2.9 μm. For comparison purposes to the frozen samples, five replicates of the fresh carrot tissue were imaged using the optimized scanning and reconstruction workflows detailed by Vicent et al. (2017).

2.6 Image processing

A preliminary analysis was carried out from the undisturbed central part of the CT images to determine the representative elementary volume (REV) based on the method proposed by Mendoza et al. (2007). The aim is to establish the minimum REV that provides representation of the macroscopic properties of the product. REV analysis is a very common and important feature in imaging and transport phenomena (Mendoza et al., 2007; Russ, 2016; Heinzl et al., 2018). Vicent et al. (2017) applied this method to frozen apple tissue to assess the REV for quantitative analysis of the 3D ice crystals during freezing at different rates. Therefore, six different volumes were subdivided from the same stack of carrot images by varying the sub-volume length to 64, 128, 280, 340, 420 and 560 pixels (8.9 μm per pixel). Thus, from each sub-volume, three stacks of images from three different samples were analyzed. Then, the average ice volume and standard deviation for three sub-volumes were computed. The analytical procedure was carried out using Avizo 9.2.0 software (FEI VSG, Bordeaux, France).

2.7 Image segmentation

In this study, the segmentation methodology developed by Vicent et al. (2017) makes it possible to segment the ice crystals in carrot by prior analysis of the X-ray attenuation coefficients of the reference model samples, as described in Section 2.4. Fig. 3a shows a μCT-

slice of frozen water representing ice at -18 ^{o}C and Fig. 3b displays a µCT-slice of concentrated carrot juice identified as representing the unfrozen-matrix in frozen carrot at -18 ^{o}C. The components in the µCT images of frozen carrot vary in density from low to high (as shown in Fig 3c). As each voxel of the µCT image may comprise one or more components. This has resulted in a large variation in intensity density ranging from 0 to 255 greyscales across the frozen carrot image is found. Thus, the small black voxels in the carrot image (Fig. 3c) were identified as representing airspaces and were easily segmented by applying a minimum local threshold value. As a result of preliminary trials, the greyscale range between 0 and 20 was assumed to represent airspace (Fig. 3c).

The greyscale intensity distributions of the reference samples, frozen water (black line as shown in Fig. 3d) and concentrated carrot juice (grey line as shown in Fig. 3d), were carefully analyzed to identify the grey levels at which the frozen phase can effectively be segmented from an unfrozen matrix in the frozen carrot. Ice (Fig. 3a) was found to have greyscale values between 10 and 130 (black line in Fig. 3d), while concentrated carrot juice (Fig. 3b) resulted in greyscale levels between 100 and 220 (grey line in Fig. 3d). As expected, the greyscale histogram of frozen carrot (dotted line in Fig. 3d) overlapped with that of the two reference samples, as it comprises both the frozen and unfrozen voxels. A preliminary test suggested that the majority of ice voxels had greyscale values between 20 and 120. Subsequently, these threshold values of 20 and 120 were applied to each REV of frozen carrot (Fig. 5b-f) to segment the ice fraction from the non-ice phase (unfrozen matrix) and air. Thus, CT greyscale images were transformed into a binary image consisting of three phases: intercellular airspace, ice and unfrozen phases.

2.8 Spatial resolution analysis

The spatial resolution of the CT image is related to the smallest feature that can be visualized or the smallest distance between two features that can be resolved. A statistical method

suggested by Hsieh (2009) was applied to identify the spatial resolution at which the objects with small density deviations can be identified. Vicent et al. (2017) used this method to detect the smallest ice crystals in the frozen apple tissue. As such, the frozen water (Fig. 3a) was subdivided into square regions of interest (ROI), with different sub-ROIs of 100, 60, 30, 20, 15, 10, 8, 6, 4, 2 and 1 voxel lengths, each with five sub-ROI replicates. From each sub-ROI, the mean intensity value was computed, and the standard deviations (σ) of the means were then calculated. These steps were also done on the concentrated carrot juice image (Fig. 3b), given that both scans were imaged under the same conditions. The mean intensity difference for objects to be distinguished was determined to be 3.29σ based on a *t*-test with 4 degrees of freedom at a 5 % significance level; σ is the standard deviation that was assumed to be the same for both frozen water and concentrated juice. We then established that a resolution of two voxels (18 µm) was the smallest resolution for which the greyscale level was still significantly different between frozen water and concentrated juice.

2.9 Quantitative data analysis

For subsequent quantitative analysis, a watershed separation was effectively utilized on binary images of the frozen phase to separate the connected ice crystals. Fig. 4 demonstrates the watershed separation procedure of frozen carrot, and the region of interest (ROI) image is presented in Fig. 4a followed by image segmentation using the attenuation coefficients of the reference samples (Fig. 3a and b). This ensured effective separation of ice crystals that were touching each other and demonstrated their size distribution. The separated ice crystals were superimposed to the original CT image (Fig. 4a) to elucidate how well the ice crystals were separated from each other (Fig. 4b). The separated ice crystals were then labeled individually as shown in Fig. 4c. This method has been applied in frozen apple tissue to distinguish ice crystals formed during freezing (Vicent et al., 2017) as well as in frozen potatoes to quantify the 3D ice crystal structure (Zhao and Takhar, 2017). To facilitate quantitative analysis, the

ice crystals intersecting the borders of the REV may generate improper structure information that needs to be excluded by using a border kill module. The separated ice crystal dataset produced by Avizo Platform were imported into Matlab (R2015a, Mathworks Inc., Natick, MA, U.S.A), where their ice size distributions were analyzed in five replicates. Lastly, a two-sample Kolmogorov-Smirnov test ($p < 0.05$) was carried out for statistical comparison of the data.

3. Results and discussion

3.1 Microstructural changes

Fig. 5a shows a µCT slice scan of fresh carrot tissue scanned at a voxel resolution of 2.9 µm. The dark spots represent airspaces, and the grey regions show the cellular matrix. Fig. 5b-f shows CT cross-section slices of the same frozen carrot sample acquired at different time points during a two-month storage period under dynamically changing temperature scenario. The intermediate grey regions probably correspond to the frozen phase in frozen carrot tissue. The bright voxels correspond to the unfrozen-matrix that comprises insoluble tissue materials and unfrozen water that was not seen in fresh tissue (Fig. 5a). This is because the frozen phase has a lower density than that of water, and the unfrozen matrix has a higher density than water and lights up in brighter interconnected lines. The µCT images clearly show a patchwork of oblong ice crystals with liquid concentrated juice in between. By comparing the µCT cross-section slices, the ice crystals visibly become larger as storage time increases (Fig. 5b-f). This can plausibly be explained by ice recrystallization occurring often during storage when temperatures fluctuate. When the frozen carrot undergoes temperature variations during frozen storage, the small ice crystals are subjected to melting-diffusion-refreezing cycles leading to crystal growth (Ndoye and Alvarez, 2015; Guo et al., 2018). Guo et al. (2018) recently revealed that the melting-refreezing mechanism is responsible for changes of ice crystal morphology in ice cream during storage under thermal variations.

These results agree with previous studies focused on ice crystal growth during frozen storage with temperature fluctuations. Ullah et al. (2014) showed that ice crystals formed in potatoes were reported to increase in size as a function of the amplitude of the temperature fluctuations and storage time. Enlargement of the ice crystals changed the potato microstructure. Zhao and Takhar (2017) investigated the evolution of ice crystal structure in frozen potatoes stored with different amplitudes of temperature fluctuations. Due to recrystallization both the ice crystal size distribution as well as their spatial distribution changed during storage (Hartel, 1998; Zaritzky, 2000; Hagiwara et al., 2006; Ndoye and Alvarez, 2015). This was shown to lead to microstructural changes in different frozen-food materials (Mousavi et al., 2007; Ullah et al., 2014). The qualitative information in the μCT images of the frozen carrot visibly prompted us to quantitatively analyze them to obtain a comprehensive insight into 3D ice crystal morphology (size, number and spatial distribution).

3.2 Representative elementary volume analysis

A representative elementary volume (REV) analysis of the ice-volume fraction was conducted on three different sub-volume images of frozen carrot. For each sub-volume, the mean ice volume fraction was computed from the ratio of ice-volume segmented divided by the total volume of the REV considered. The results showed no statistical differences between the mean ice-volume fractions computed from the different sub-volumes as shown in Fig. 6. However, a trend was identified: it was observed that the standard deviation decreased as the sub-volume size increased. For the smallest sub-volume size of 0.18 mm^3, the computed standard deviation was 2.07 % compared with 1.41 % for a sub-volume size of 1.48 mm^3. The statistical data show the variability to decrease as the sub-volume (REV) increases. The largest sub-volume selected, i.e., 123.8 mm^3, had a standard deviation as small as 0.53 %. Sub-volumes larger than 123.8 mm^3 were not considered because they may include the carrot sample boundaries, which may be damaged during preparation, resulting in different

297 macroscopic structures of the analyzed sub-volume sample. The results indicate that a REV of
298 340 × 340 × 340 voxels equivalent to a volume of 27.71 mm^3, showed no appreciable
299 difference in the standard deviation with the largest sample volume as shown in Fig. 6.
300 Therefore, this REV was selected as the best for each set of images for further quantitative
301 analysis to provide representation of the macroscopic properties of the frozen carrot.

302 **3.3 Ice crystal quantification**

303 To facilitate quantitative analysis, a watershed separation was applied to separate the
304 connected ice crystals as described in Section 2.9. Table 1 shows the quantitative parameters
305 of ice crystals, including crystal size distribution, the mean ice crystal count and the mean
306 equivalent diameter analyzed in five replicates for each time point. For comparison purposes,
307 these mean values for each parameter were statistically analyzed over a two-month storage
308 period under dynamically changing temperature. At 0 d a large number (N = 1980 ± 80) of
309 small crystals were found with a mean equivalent diameter equal to 246 ± 15.9 µm (Table 1).
310 This value concurs well with those of Voda et al. (2012) and van der Sman et al. (2013). Both
311 studies considered carrot tissue during freezing at -28 ^{o}C and reported the ice crystal sizes of
312 239 µm and 241 µm, respectively. After 7 d of storage under dynamically changing
313 temperature, the mean equivalent diameter increased to 342 ± 13.2 µm while the average
314 crystal count decreased to N = 1650 ± 60 (Table 1). During further storage the mean
315 equivalent diameter and number of ice crystals continued to increase and decrease,
316 respectively, until 60 d the mean equivalent crystal diameter was as much as 578 ± 27.6 µm
317 with a reduction in the total number of ice crystals to N = 670 ± 160 (Table 1). Until 30 d the
318 mean equivalent diameter of the ice crystals was found to be significantly different at every
319 subsequent storage time (p < 0.05), but not after 30 d. Similar conclusions could be drawn
320 with respect to the number of ice crystals. The number of ice crystal decreased during 30 d of
321 storage, presumably because smaller crystals melted and refroze on larger crystals. This

322 decreasing trend in the ice crystal count was noted during 30 d period of storage. After 30 d
323 no further significantly changes in the total number of ice crystals were observed. In addition,
324 the median equivalent diameter of the ice crystals increased from 236 ± 24.8 µm, to 305 ±
325 20.0 µm, 385 ± 23.2 µm, 508 ± 43.6 µm and 544 ± 220 µm at 0 d, 7 d, 14 d, 30 d and 60 d of
326 storage, respectively (Table 1).
327 Several studies have shown similar ice crystal growth during storage, especially in a context
328 of temperature abuse. Ullah et al. (2014) and Zhao and Takhar (2017) worked with frozen
329 potatoes during storage under temperature fluctuations over a 30 d period. Ullah et al. (2014)
330 reported a mean equivalent ice crystal diameter of 284.34 µm in the control potato samples
331 stored at -80 ^{o}C. During a storage period of 10 d at fluctuating temperatures ranging from -17
332 ^{o}C to -16 ^{o}C, the mean crystal diameter increased to 431.89 µm. When the amplitude of
333 temperature fluctuations increased from -17 ^{o}C to -11 ^{o}C for the next 10 d, the mean crystal
334 size increased to 593.07 µm. Finally, a larger mean equivalent diameter of 605.03 µm was
335 reported following large temperature fluctuations of -17 ^{o}C to -7 ^{o}C during the last 10 d of
336 storage. Zhao and Takhar (2017) reported a mean equivalent diameter of 112.66 µm in a
337 control potato sample at -80 ^{o}C and showed a growth trend in the mean crystal size during
338 storage. Samples stored at -17 ^{o}C to -16 ^{o}C for 14 d showed a mean equivalent diameter of
339 223.35 µm. The ice crystal size grew to 508.01 µm in potato samples stored at -17 ^{o}C to -11
340 ^{o}C for the next 14 d. Large ice crystals with a mean size of 832.84 µm were found after 14 d
341 of storage with a large amplitude of fluctuating temperatures from -17 ^{o}C to -7 ^{o}C. The
342 authors suggested that ice crystal growth is due to the smaller crystals merging with large ice
343 crystals, and this process was influenced by temperature fluctuations. A reduction in the total
344 number of ice crystals was also stated.
345 The difference between mean ice crystal sizes reported in the literature for frozen potatoes
346 and in this work for carrots might be due to the differences in histology. Mousavi et al. (2007)

showed that different food materials (carrot and potato) produce different ice crystal morphology as well as different microstructure during freezing. Ullah et al. (2014) also reported different ice crystal data in potatoes during storage under stepwise increasing temperature fluctuations, which was concurred by the results of Zhao and Takhar (2017). In our study we investigated scenarios with regular pulse like temperature changes. The differences in ice crystal size and number between our study and that of Ullah et al. (2014) may be a consequence of the different temperature profiles or differences in materials properties of potato and carrot tissue. For example, the viscosity of the unfrozen phase depends on its chemical composition and determines how fast water diffuses towards the ice nuclei, thus defining the recrystallization rate.

The results of the current study revealed that the mean size of ice crystals increased in frozen carrot during one month of storage with dynamically changing temperature, while the total number of the ice crystal decreased accordingly. The rise in temperature from -18 ^{o}C to -5 ^{o}C during dynamic storage likely influenced molecular mobility and ice recrystallization as water molecules in small crystals are more weakly bound than in large crystals (Hartel, 1998; Hagiwara et al., 2006).

Donhowe and Hartel (1996) showed a similar trend of ice crystal growth in ice cream during bulk storage under temperature fluctuations. We believe that the enlargement of ice crystals in carrot in our experiments was due to the Ostwald ripening mechanism occurring during frozen storage. However, the ice crystal growth rate that we observed in frozen carrot was less than those reported for ice cream by Donhowe and Hartel (1996). The extent to which ice crystals grow in carrot could be explained by the presence of the cell wall, which might acts as a structural barrier for ice recrystallization. The cell walls are composed of cellulose microfibrils, pectin, hemicellulose and glycoproteins embedded in a highly cross-linked matrix of polysaccharide (Préstamo et al., 1998). In this way, the water molecules can be

trapped by these network structures of the unfrozen matrix and forms a gel-like structure (Waldron et al., 2003; Agoda-Tandjawa et al., 2012). This may alter the rheological behavior and reduce the molecular mobility of water. This may also explain why the rate of ice recrystallization is faster in ice cream, which does not have cell walls or equivalent microstructural features.

The physical state of the food products at sub-zero temperatures is strongly correlated to the glass transition temperature (T_g'). T_g' of the product refers to the transformation point of the product matrix into a glassy state, i.e., at a temperature below T_g'. The molecular mobility of the material then becomes extremely slow due to high viscosity. In a glass state, the undesirable changes that are diffusion-controlled, such as ice-recrystallization are greatly restricted. Generally, frozen foods stored at a temperature below T_g' are considered highly stable (Fennema, 1996; Reid, 1998; Roos, 1998), and therefore have a high storability. In contrast, in the rubbery state, i.e., at a temperature above T_g' and below the freezing point, the viscosity decreases and the molecular mobility increases (Goff, 1992, 1994; Goff et al., 1993; Reid, 1998; Roos, 1998). Changes of ice crystals can occur and lead to microstructure alteration and subsequently affect quality during storage. The rate of diffusion-controlled phenomena, such as ice crystal growth is highly related to the magnitude of the temperature difference, and increases exponentially with increasing temperature difference according to the Williams-Landel-Ferry theory (Sutton et al., 1996; Ablett et al., 2002). Hence, the proximity to the glass transition temperature of the product describes the rate at which ice recrystallization proceed. Gonçalves et al. (2007) measured the glass transition temperature in carrot to be approximately -32 ^{o}C. This suggests that during our dynamic storage experiments, the carrot samples were in the rubbery state and subject to diffusion phenomena.

3.4 Ice crystal size distributions

The ice crystal size distribution was analyzed in five replicate carrot samples and was found to be significantly different ($p < 0.05$) for each time point (Fig. 7). There was a significant shift in ice crystal size distribution to larger crystal sizes for each time point during two months of storage under dynamically changing temperature. The carrot samples after freezing and before storage, i.e., at 0 d, shows a much smaller ice crystal size distribution ranging from 20 to over 590 μm (dotted line in Fig. 7) and the range was narrower than that of the stored carrot samples. During storage, a gradual change in ice crystal size distribution was observed. The results clearly revealed that the crystal size distributions become broader as storage time increases, in line with the changes of mean crystal size reported in Section 3.3. Larger ice crystals were formed over a long period of storage with dynamically changing temperature, and lead to microstructural changes of carrot tissue structure. Analogous to ice crystal size distribution in frozen carrot, Mousavi et al. (2007) showed a larger ice crystal size distribution ranging from 400 to 1200 μm during freezing at -5 ^{o}C. The ice crystal size distribution reported by Mousavi et al. (2007) in carrot differs from ours immediately after freezing, i.e., at 0 d. This is because Mousavi et al. froze carrot samples at a slow freezing rate of 0.8 ^{o}C per min as compared to the fast freezing rate of 9.1 ^{o}C per min that we employed. In a previous article (Vicent et al., 2017) we showed that different freezing rates produced different frozen apple tissue microstructures, as well as different ice crystal distributions. Larger crystals are formed during slow freezing rates, whereas fast freezing rates produce relatively smaller ice crystals. Voda et al. (2012) showed that carrot tissue frozen at -28 ^{o}C had an ice crystal size distribution ranging between 10 and 1000 μm. However, no other data on ice crystal size distribution changes in frozen carrot during storage were found in the literature.

3.5 3D microstructure of ice crystals

Fig. 8 shows the 3D models of the crystal size classes in carrot during a two-month period of storage under dynamically changing temperature. The separated ice crystals were assigned to different labels to elucidate different size classes throughout storage. 3D volume renderings of the isolated ice crystal data evidently show an increase in ice crystal size as a function of storage time. At 0 d crystals are small but they grow while becoming less in number as storage time increases. Large ice crystals clearly grow at the expense of small crystals during storage under dynamically changing temperature. Ice crystal growth may cause cell rupture and thus degrade quality. This reduces storage life and commercial value of the product during the cold chain. Vicent et al. (2018) reported that quality changes (i.e., drip loss) in frozen apple tissue were due to ice recrystallization during storage with temperature fluctuations. 3D X-ray µCT imaging of ice crystals in carrot tissue provided a unique and noninvasive means of visualizing and quantifying ice crystal growth during dynamic storage. This is in contrast to the imaging approach that has been utilized in the literature (Mousavi et al., 2007; Ullah et al., 2014; Zhao and Takhar, 2017). These authors assumed that void structures formed in freeze-dried food materials represented the ice crystal morphology. However, Voda et al. (2012) showed that the freeze-drying process may possibly impair the microstructure of frozen foods through shrinkage. Also, it is difficult to make a distinction between the air pores that were present in the unfrozen sample and those were created by the freeze-drying process due to dehydration of the cells. This leads to errors in the estimation of the ice crystal size, shape and spatial distribution. Freeze-drying thus may yield inconsistent and incomplete results.

3.6 Pore analysis

For comparison purposes, the pore structures in fresh and frozen carrot samples were quantified based on the optimized greyscale level for airspaces as discussed in Section 2.7.

Fig. 5b-f clearly show a smaller pore size in frozen carrot scans compared with that of fresh carrot (Fig. 5a). Fresh samples had a mean pore equivalent diameter of 38.43 ± 2.81 µm with mean pore sphericity, i.e., shape factor of 0.89 ± 0.04. Frozen samples (0 d) had a smaller mean pore diameter of 29.70 ± 2.44 µm, with a mean pore sphericity of 0.81 ± 0.06. No significantly changes between mean pore equivalent diameters were found for each time point during storage, and also the frozen carrots showed no difference in mean pore sphericity. Small pore sizes in frozen samples may be attributed to ice formation that has larger specific volume than water. This expands into the intracellular space leads to shrinkage and may distort the airspaces. This is similar to the results reported by Vicent et al. (2017) for apple tissue during freezing at the different rates. The authors showed that the pore sizes become narrower regardless of the different freezing conditions employed. The low contrast between cell walls and intracellular materials in the fresh carrot sample inevitably leads to the inability to segment cells. Voda et al. (2012) found cell diameters in carrot ranging from 20 to 100 µm. The authors suggested that the cells' size varied depending on the age of the carrot. van Dalen et al. (2013) showed that after freezing at -28 ^{o}C the mean cell length was 100 µm compared to a maximum crystal length size of 3000 µm.

Vegetables, including carrot are microstructured and consist of cells, interconnected cell walls and intercellular airspaces of different sizes and shapes (Voda et al., 2012; van Dalen et al., 2013). Microstructural organization has been recognized as one of the key elements in describing quality and stability of foods (Aguilera, 2005; Ho et al., 2013). The frozen vegetables industry is often faced with temperature abuse scenarios that lead to ice recrystallization. Enlargement of ice crystals in carrot cortex tissue damages tissue and cell structures, thus decreases the water-holding capacity and causing the water-soluble nutrients to leach out during thawing. This affects the product microstructure and ultimately impairs storage life and food quality, such as drip loss, sensory and textural changes as well as

nutritional value (Agnelli and Mascheroni, 2002; Cruz et al., 2009; Gonçalves et al., 2011a, 2011b; Vicent et al., 2018). To minimize these undesirable changes the temperature variations throughout frozen storage and distribution should be controlled.

The results presented in this study show that our proposed imaging provides 3D ice crystal structure information of frozen foods, providing new quantitative data on carrot. In our previous work, we developed the 3D imaging based analysis to visualize and quantify the 3D microstructure and ice crystal distribution after the freezing process (Vicent et al., 2017). Here the method was used to investigate changes of ice crystals in carrot tissue during storage and showed important process-microstructure-interactions in this vegetable.

Food engineers will thus take home from this work that 3D ice crystal analysis is possible and useful to understand frozen vegetable microstructure by nondestructive means. It is an important additional technique for assessing vegetable quality during frozen storage and distribution, which was previously missing. With this work we see evidence of mechanisms of ice crystal growth as well as decrease of the number of ice crystals, which concurs with earlier theoretical work. In our opinion such data is very scarce today and of great interest to the food engineering community.

4. Conclusion

In this work, ice recrystallization phenomenon was investigated by analyzing the 3D ice crystal count and size distributions in frozen carrot tissue using X-ray µCT under dynamically changing temperature. The ice crystal size distributions was found to become broader for each time point with an increase in the size of ice crystals. Moreover, a reduction in the total number of ice crystals was observed in carrot during a two-month storage period. It can be concluded that X-ray µCT provides a vast potential to image the 3D microstructure of ice

crystals without significant preparation of the sample. It can thus be used for quality-control processes of frozen vegetables in the cold storage and distribution sector.

Quantitative data sets obtained from the 3D imaging of ice crystals are also useful for modeling purposes at the microscopic level to acquire a better understanding of the microstructural changes induced at the macroscopic scale. Such a model, describing the population ice crystal size distribution and energy balance, will be developed to better understand and predict ice recrystallization, which is linked to the microstructural and quality changes in plant-based food materials during frozen storage under temperature abuse conditions.

Acknowledgement

The authors wish to thank DIM ASTREA (as proposed by the Regional Council of Ile-de-France, France) for financial support under Award No. Ast 140054, 2014. They also acknowledge financial support from the KU Leuven (project C16/16/002, KA/16/057) and VLAIO (IWT 140992).

/References

Ablett, S., Clarke, C.J., Izzard, M.J., Martin, D.R., 2002. Relationship between ice recrystallisation rates and the glass transition in frozen sugar solutions. *Journal of the Science of Food and Agriculture, 82(15),* 1855-1859.

Agnelli, M.E., Mascheroni, R.H., 2002. Quality evaluation of foodstuffs frozen in a cryomechanical freezer. *Journal of Food Engineering, 52(3),* 257-263.

Agoda-Tandjawa, G., Durand, S., Gaillard, C., Garnier, C., Doublier, J.L., 2012. Properties of cellulose/pections composites: Implications for structural and mechanical properties of cell wall. *Carbohydrate Polymers, 90 (2),* 1081-1091.

Aguilera, J.M., 2005. Why food microstructure? *Journal of Food Engineering, 67(1),* 3-11.

515 Aguilera, J.M., Stanley, D.W., 1999. Food structuring. In: Aguilera, J.M., Stanley, W.D.
516 (Eds.), *Microstructural Principles of Food Processing and Engineering*, 2nd ed. Aspen
517 Publishers, Inc, Gaithersburg, Maryland, pp. 238-244.
518 Bogh-Sorensen, L., 2006. Recommendations for the processing and handling of frozen, 4th
519 ed. Paris: *International Institute of Refrigeration* (IIR), pp. 8-10.
520 Cruz, R.M.S., Vieira, M.C., Silva, C.L.M., 2009. Effect of cold chain temperature abuses on
521 the quality of frozen watercress (*Nasturtium officinale* R. Br.). *Journal of Food*
522 *Engineering, 94(1)*, 90-97.
523 Donhowe, D.P., Hartel, R.W., 1996. Recrystallization of ice during bulk storage of ice cream.
524 *International Dairy Journal, 6(11-12)*, 1209-1221.
525 Fennema, O.R., 1996. Water and ice. In: Fennema, O., (Ed.), *Food Chemistry*, 3rd ed. New
526 York: Marcel Dekker, pp. 17-94.
527 Goff, H.D., 1992. Low-temperature stability and the glassy state in frozen foods. *Food*
528 *Research International, 25(4)*, 317-325.
529 Goff, H.D., 1994. Measuring and interpreting the glass transition in frozen foods and model
530 systems. *Food Research International, 27(2)*, 187-189.
531 Goff, H.D., Caldwell, K.B., Stanley, D.W., Maurice, T.J., 1993. The influence of
532 polysaccharides on the glass transition in frozen sucrose solutions and ice cream.
533 *Journal of Dairy Science, 76(5)*, 1268-1277.
534 Gonçalves, E.M., Abreu, M., Brandão, T.R.S., Silva, C.L.M., 2011a. Degradation kinetics of
535 colour, vitamin C and drip loss in frozen broccoli (*Brassica oleracea* L. ssp. Italica)
536 during storage at isothermal and non-isothermal conditions. *International Journal of*
537 *Refrigeration, 34(8)*, 2136-2144.
538 Gonçalves, E.M., Lopes, C., Pinheiro, J., Lourenco, J.A.A., Abreu, M., Brandão, T. R.S.,

539 Silva, C.L.M., 2007. Differential scanning calorimetry as a tool for optimizing
540 vegetables freezing and storage conditions. *In EFFost/EHEDG Joint National*
541 *Conference*, Lisbon, Portugal, 14-16 November, 2007.

542 Gonçalves, E.M., Pinheiro, J., Abreu, M., Brandão, T.R.S., Silva, C.L.M., 2011b. Kinetics of
543 quality changes of pumpkin (*Curcurbita maxima* L.) stored under isothermal and non-
544 isothermal frozen conditions. *Journal of Food Engineering, 106(1)*, 40-47.

545 Guo, E., Kazantsev, D., Mo, J., Bent, J., Van Dalen, G., Schuetz, P., Rockett, P., StJohn, D.,
546 Lee, P.D., 2018. Revealing the microstructural stability of a three-phase soft solid (ice
547 cream) by 4D synchrotron X-ray tomography. *Journal of Food Engineering, 237*, 204-
548 214.

549 Hagiwara, T., Hartel, R.W., Matsukawa, S., 2006. Relationship between Recrystallization
550 Rate of Ice Crystals in Sugar Solutions and Water Mobility in Freeze-Concentrated
551 Matrix. *Food Biophysics, 1(2)*, 74-82.

552 Hartel, R.W., 1998. Mechanisms and kinetics of recrystallization in ice cream. In: Reid, D.S.
553 (Ed.), *The Properties of Water in Foods*. Springer US, Boston, MA, pp. 287-319.

554 Heinzl, C., Amirkhanov, A. and Kastner, J., 2018. Processing, Analysis and Visualization of
555 CT Data. In: Carmignato, S., Dewulf, W., Leach, R. (Eds.), *Industrial X-Ray Computed*
556 *Tomography*. Springer, Cham, pp. 99-142.

557 Ho, Q.T., Carmeliet, J., Datta, A.K., Defraeye, T., Delele, M.A., Herremans, E., Opara, L.,
558 Ramon, H., Tijskens, E., van der Sman, R., Van Liedekerke, P., Verboven, P., Nicola ï,
559 B.M., 2013. Multiscale modeling in food engineering. *Journal of Food Engineering,*
560 *114(3)*, 279-291.

561 Hsieh, J., 2009. Computed Tomography: Principles, Design, Artifacts, and Recent Advances,
562 2nd ed. SPIE Press, Bellingham, Washington, USA, pp. 158-159.

563 Mendoza, F., Verboven, P., Mebatsion, H.K., Kerckhofs, G., Wevers, M., Nicolaï, B., 2007.
564 Three-dimensional pore space quantification of apple tissue using X-ray computed
565 microtomography. *Planta, 226(3)*, 559-570.

566 Mousavi, R., Miri, T., Cox, P.W., Fryer, P.J., 2007. Imaging food freezing using X-ray
567 microtomography. *International Journal of Food Science and Technology, 42(6)*, 714-
568 727.

569 Ndoye, F.T., Alvarez, G., 2015. Characterization of ice recrystallization in ice cream during
570 storage using the focused beam reflectance measurement. *Journal of Food Engineering,*
571 *148*, 24-34.

572 Préstamo, G., Fuster, C. and Risueño, M.C., 1998. Effects of blanching and freezing on the
573 structure of carrots cells and their implications for food processing. *Journal of the*
574 *Science of Food and Agriculture, 77(2)*, 223-229.

575 Pronk, P., Infante Ferreira, C.A., Witkamp, G.J., 2005. A dynamic model of Ostwald ripening
576 in ice suspensions. *Journal of Crystal Growth, 275(1-2)*, 1355-1361.

577 Reid, D.S., 1998. Crystallization phenomena in the frozen state. In: Rao, M.A., Hartel, R.W.
578 (Eds.), *Phase/state Transition in Foods: Chemical, Structural, and Rheological Changes*.
579 Marcel Dekker, Inc., New York, pp. 312-326.

580 Reid, D.S., Kotte, K., Kilmartin, P., Young, M., 2003. A new method for accelerated shelf-
581 life prediction for frozen foods. *Journal of the Science of Food and Agriculture, 83(10)*,
582 1018-1021.

583 Roos, Y.H., 1998. Role of water in phase-transition phenomena in foods. In: Rao, M.A.,
584 Hartel, R.W. (Eds.), *Phase/state Transition in Foods: Chemical, Structural, and*
585 *Rheological Changes*. Marcel Dekker, Inc., New York, pp. 57-86.

586 Russ, J.C., 2016. 3D Visualization. In: *The Image Processing Handbook*. 6th ed. CRC press,

587 Boca Raton, FL, pp. 707-763.

588 Sutton, R.L., Lips, A., Piccirillo, G., Sztehlo, A., 1996. Kinetics of Ice Recrystallization in
589 Aqueous Fructose Solutions. *Journal of Food Science, 61(4),* 741-745.

590 Syamaladevi, R.M., Manahiloh, K.N., Muhunthan, B., Sablani, S.S., 2012. Understanding the
591 Influence of State/Phase Transitions on Ice Recrystallization in Atlantic Salmon (*Salmo*
592 *salar*) During Frozen Storage. *Food Biophysics, 7(1),* 57-71.

593 Ullah, J., Takhar, P.S., Sablani, S.S., 2014. Effect of temperature fluctuations on ice-crystal
594 growth in frozen potatoes during storage. *LWT - Food Science and Technology, 59(2),*
595 1186-1190.

596 van Dalen, G., Koster, M., Nijsse, J., Boller, E., van Duynhoven, J., 2013. 3D imaging of
597 freeze-dried vegetables using X-ray microtomography, *Proceedings of the Micro-CT*
598 *user meeting SkyScan*, Hasselt, Belgium, 15-18 April, 2013.

599 van der Sman, R.G.M., Voda, A., van Dalen, G., Duijster, A., 2013. Ice crystal interspacing in
600 frozen foods. *Journal of Food Engineering, 116(2),* 622-626.

601 Vicent, V., Ndoye, F.T., Verboven, P., Nicolaï, B., Alvarez, G., 2018. Quality changes
602 kinetics of apple tissue during frozen storage with temperature fluctuations.
603 *International Journal of Refrigeration, 92,* 165-175.

604 Vicent, V., Verboven, P., Ndoye, F.T., Alvarez, G., Nicolaï, B., 2017. A new method
605 developed to characterize the 3D microstructure of frozen apple using X-ray micro-CT.
606 *Journal of Food Engineering, 212,* 154-164.

607 Voda, A., Homan, N., Witek, M., Duijster, A., van Dalen, G., van der Sman, R., Nijsse, J.,
608 van Vliet, L., Van As, H., van Duynhoven, J., 2012. The impact of freeze-drying on
609 microstructure and rehydration properties of carrot. *Food Research International, 49(2),*
610 687-693.

611 Waldron, K.W., Parker, M.L., Smith, A.C., 2003. Plant and Cell Walls and Food Quality.
612 *Comprehensive Reviews in Food Science and Food Safety*, *2(4)*, 128-146.
613 Zaritzky, N.E., 2000. Factors affecting the stability of frozen foods. In: Kennedy, C.J. (Ed.),
614 *Managing Frozen Foods*. Woodhead Publishing, pp. 111-135.
615 Zhao, Y., Takhar, P.S., 2017. Micro X-ray computed tomography and image analysis of
616 frozen potatoes subjected to freeze-thaw cycles. *LWT - Food Science and Technology*,
617 *79*, 278-286.

618

Figure and Table captions

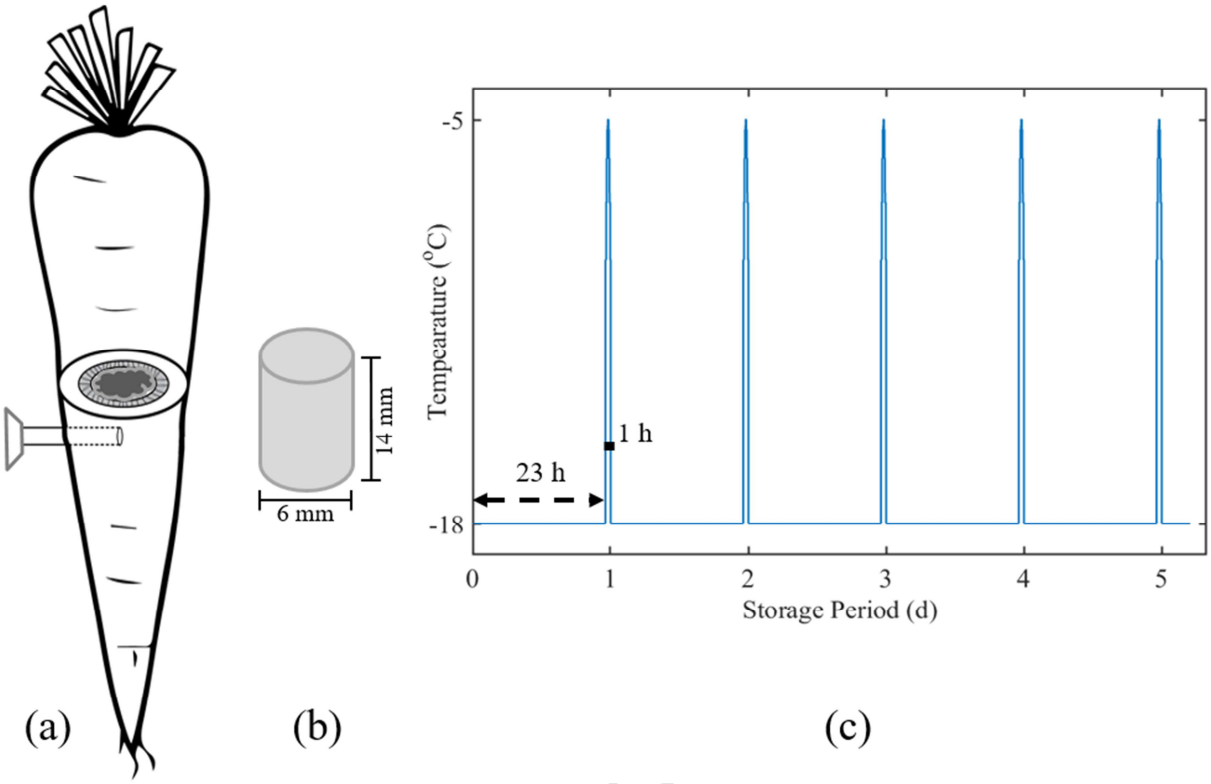

Fig. 1. **(a)** A simplified schematic representation showing the different regions of carrot tissue (parenchyma cells, vascular tissue and peripheral cortex tissue). **(b)** Excision of the cylindrical carrot samples for μCT imaging, excluding the core region (parenchyma cells). The air-temperature profile shows a dynamically changing condition during a two-month period of frozen storage **(c)**.

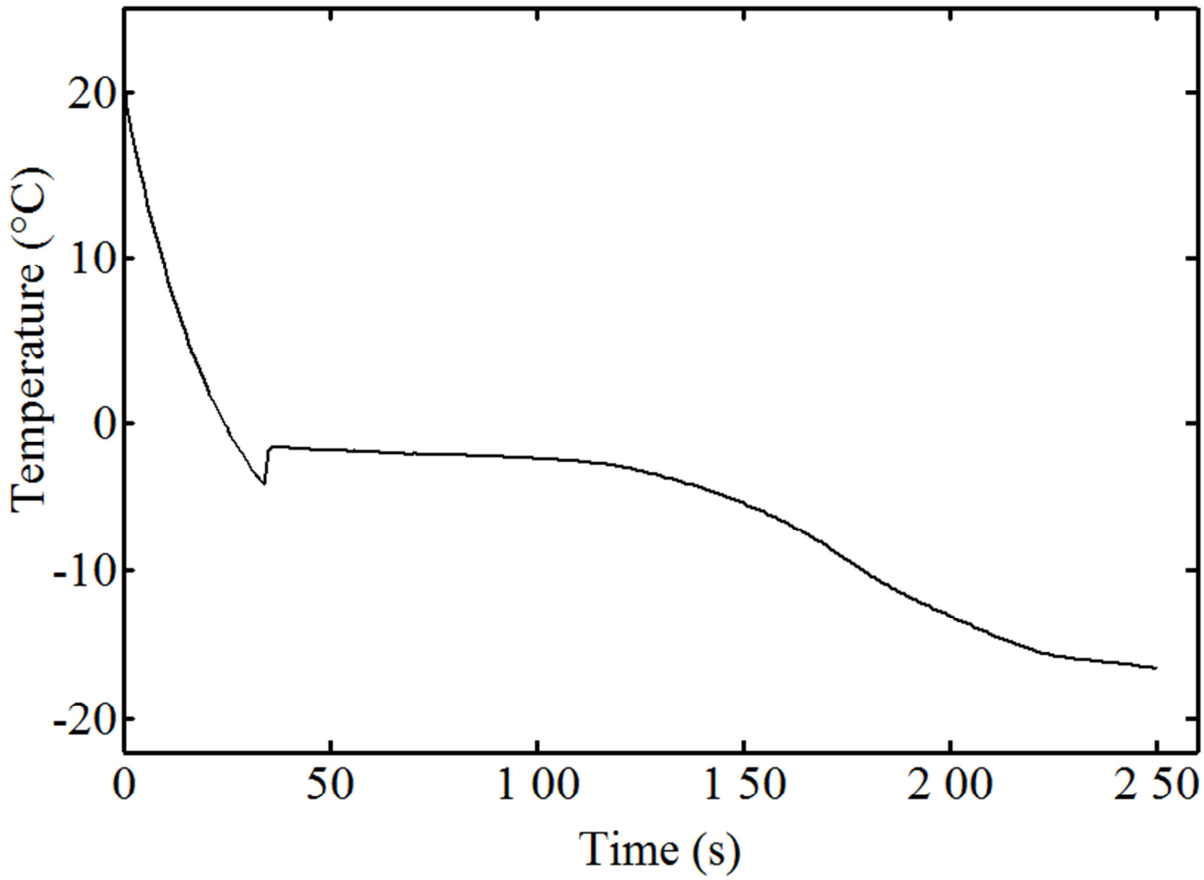

Fig. 2. Freezing curve demonstrates the different steps during freezing process of the carrot tissue samples.

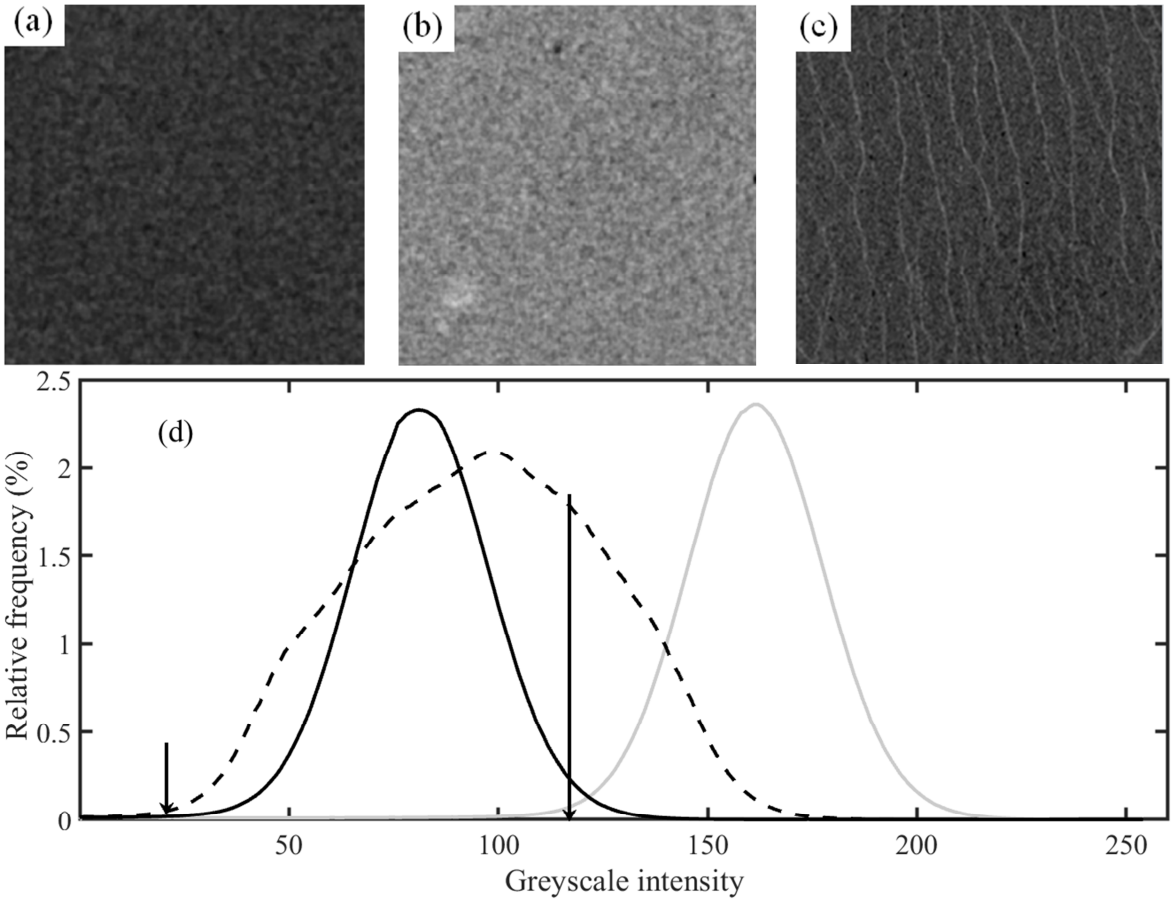

Fig. 3. CT cross-section slices of frozen water (**a**), concentrated carrot juice stored at -18 ^{o}C (**b**), and frozen carrot (**c**) imaged using X-ray Computed Tomography with a voxel resolution of 8.9 μm. (**d**) shows the greyscale intensity histogram of frozen water (black line), concentrated carrot juice (grey line) and frozen carrot (dotted line). The threshold values of 20 and 120 (shown by the two arrows) were applied to the CT images of the carrots to label voxels as frozen, unfrozen and air.

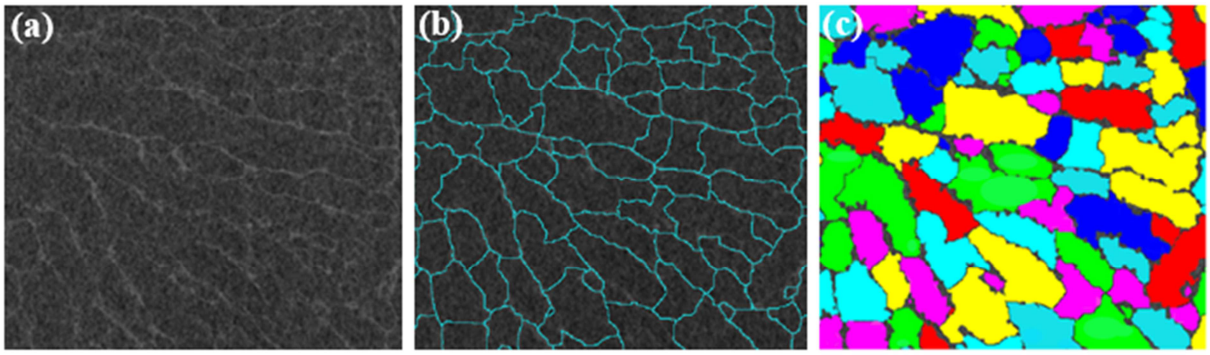

Fig. 4. Image processing procedure implemented in Avizo (Image analysis software) for the µCT image of frozen carrot tissue. (**a**) Region of Interest (ROI) image followed by image segmentation using the attenuation coefficients of the reference samples, (**b**) separated ice crystals using the watershed separation module, and (**c**) labeling of separated ice crystals.

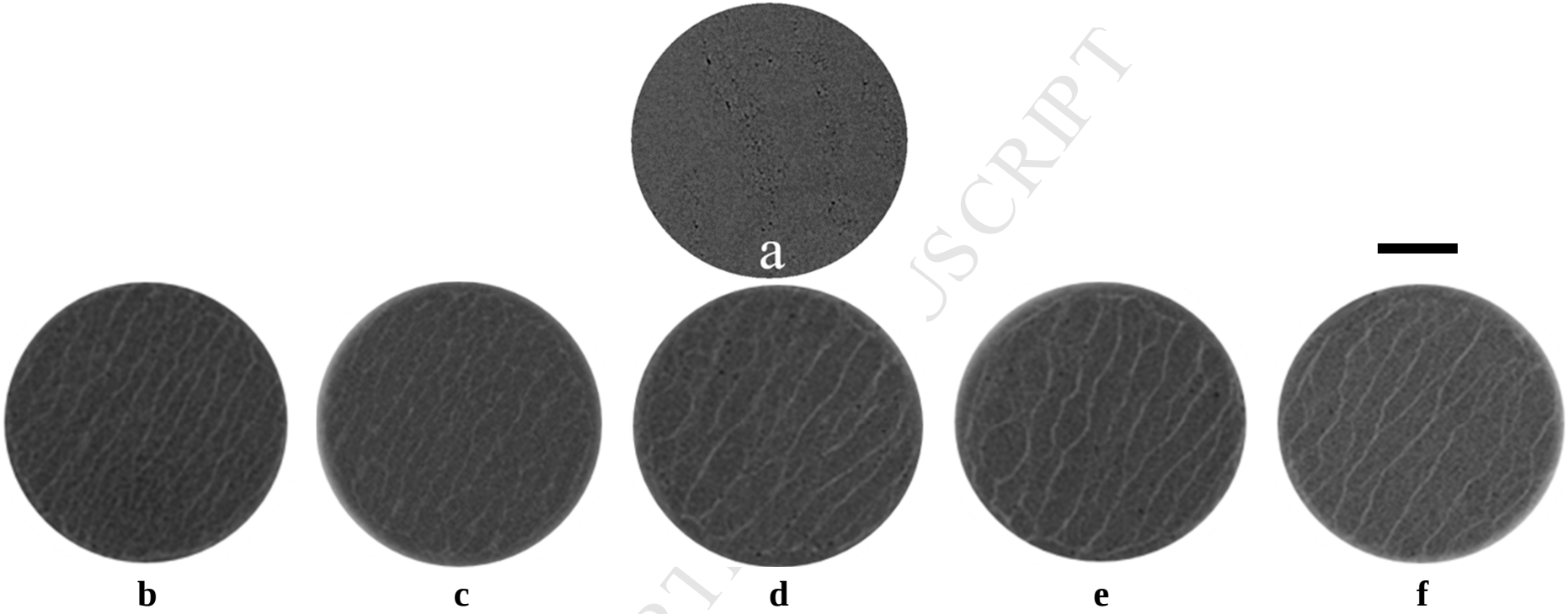

Fig. 5. µCT slice of fresh carrot tissue (**a**); the black voxels represent airspaces, the grey voxels correspond to cells. CT cross-section slices of the same frozen carrot sample after freezing at 0 d (**b**), and during 7 d (**c**), 14 d (**d**), 30 d (**e**) and 60 d (**f**) of storage under dynamically changing temperature. The black voxels represent the airspaces. The dark grey regions correspond to ice crystals, and the light grey voxels denote the unfrozen matrix. Fresh carrot was scanned using a Skyscan 1172 CT system at a voxel resolution of 2.9 µm; frozen samples were imaged using X-ray µCT (DeskTom RX 130) at a voxel resolution of 8.9 µm. The scale bar represents 2000 µm.

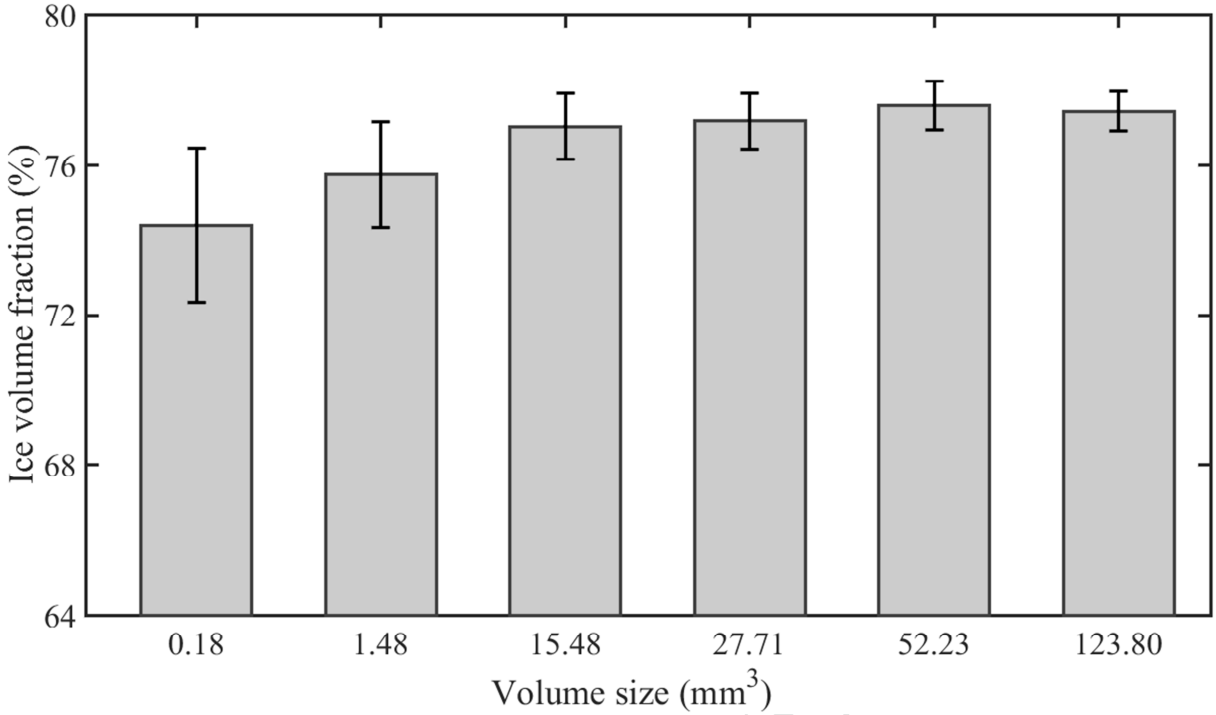

Fig. 6. Histogram plot shows the mean ice-volume fractions for the different sub-volume sizes analyzed to compute the representative elementary volume (REV). The mean data were analyzed in triplicate stacks of images of frozen carrot. Error bars indicate the standard errors of the calculated mean ice volume fraction.

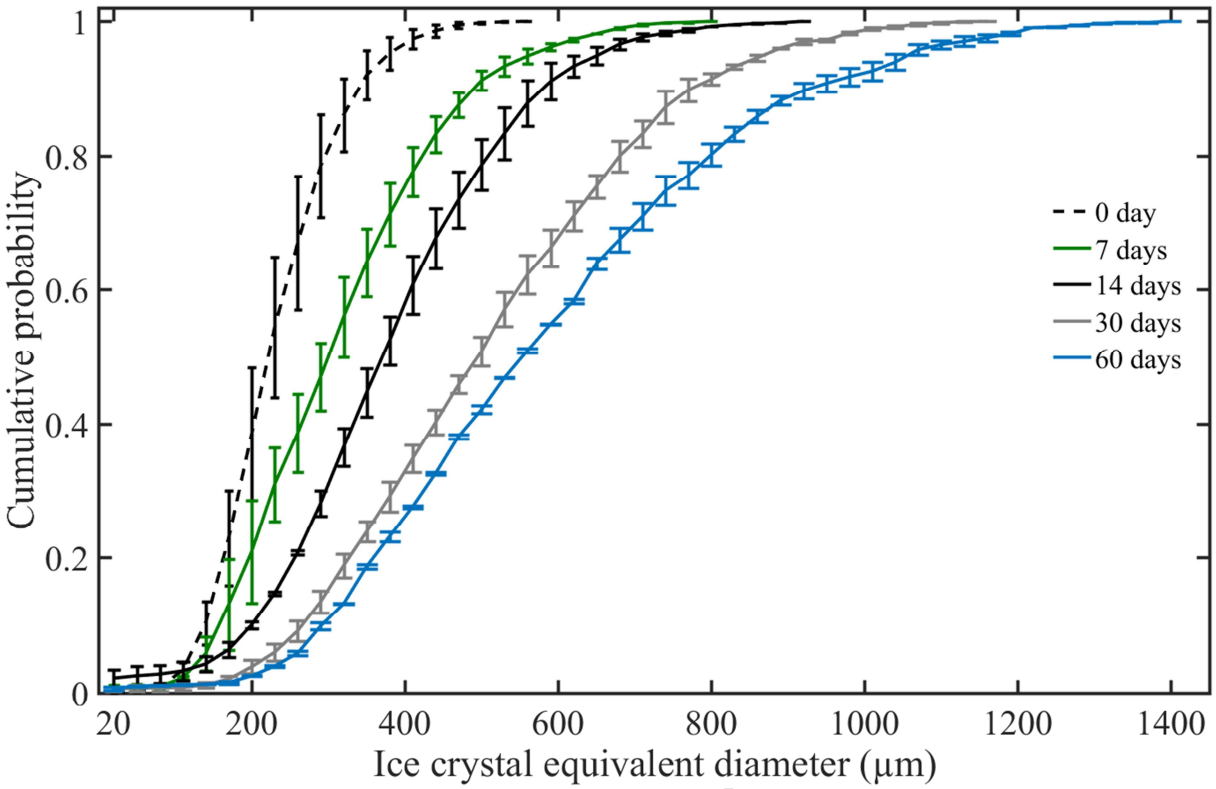

Fig. 7. Ice crystal size distribution in frozen carrot samples stored under dynamically changing temperature during a two-month period. The cumulative distribution data were based on the analysis of five replicates for each time-point. The sample size was 340 × 340 × 340 voxels at a voxel size of 8.9 μm^3.

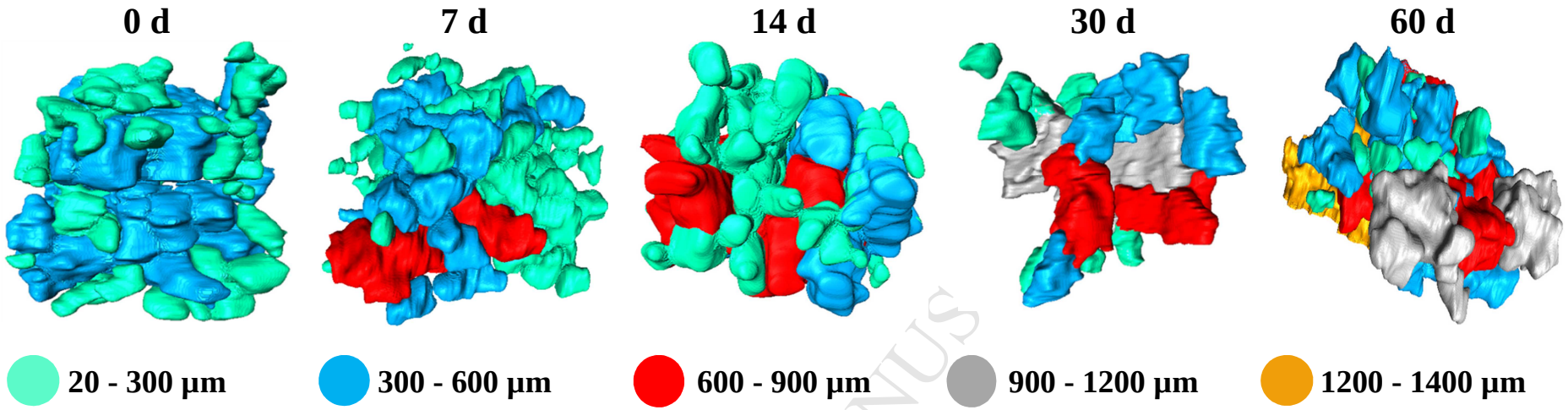

Fig. 8. 3D volume renderings of the isolated ice crystal data of the same carrot tissue sample stored under dynamically changing temperature scenarios over a two-month storage period. Ice crystals were segmented and separated according to the imaging analysis suggested by Vicent et al. (2017). Ice crystals were subsequently and individually labeled based on their equivalent diameters to describe the different size classes. The 3D models represent 240 × 240 × 240 voxels at a voxel size of 8.9 μm^3.

Table caption

Table 1

Ice crystal size distribution, mean equivalent diameter, median equivalent diameter and mean number of ice crystals during a two-month period of storage with dynamically changing temperature. Mean and median values of the separated ice crystals in carrot were based on the analysis of five replicate samples of images for each time point. Mean and median values are represented with their standard deviations ($\bar{x} \pm$ S.D.), values with different superscripts for each parameter indicate that the means are significantly different at ($p < 0.05$).

Storage time (d)	Ice crystal size range (µm)	Mean equivalent diameter (µm)	Median equivalent diameter (µm)	Mean number of crystals
0	20 - 590	246 ± 15.9^{a}	236 ± 24.8^{a}	1980 ± 80^{a}
7	20 - 815	342 ± 13.2^{b}	305 ± 20.0^{b}	1650 ± 60^{b}
14	20 - 940	394 ± 18.5^{c}	385 ± 23.2^{c}	1450 ± 100^{c}
30	20 - 1170	525 ± 28.0^{d}	508 ± 43.6^{d}	940 ± 120^{d}
60	20 - 1450	578 ± 27.6^{d}	544 ± 22.0^{d}	670 ± 160^{d}

Highlights

- X-ray μCT imaging was performed to visualize the 3D ice crystal growth during storage.
- Ice crystal size increases with increase storage time under dynamic temperatures.
- Number of ice crystals decreased over a period of storage
- 3D image analysis to quantify ice crystal changes in carrot tissue during storage.